2025 IEEE World Haptics Conference (WHC)
Suwon Convention Center, Suwon, Korea
July 8 ~ 11, 2025

Ultrasound-Driven Wearable Haptic Display for Rendering Edges and Curved Surfaces

Tao Morisaki[1], Aoba Sekiguchi[2], Takaaki Kamigaki[2], Yasutoshi Makino[2], Hiroyuki Shinoda[2]
(1) NTT Communication Science Laboratories, NTT, Inc. Atsugi, Japan
(2) Dept. of Complexity Science and Engineering, The University of Tokyo, Kashiwa, Japan
tao.morisaki@ntt.com,
{sekiguchi, kamigaki}@hapis.k.u-tokyo.ac.jp, {yasutoshi_makino, hiroyuki_shinoda}@k.u-tokyo.ac.jp

***Abstract*—Haptic local features such as edge and surface curvature are fundamental components that form haptic experiences. Noncontact haptic displays using focused ultrasound can render such local features by precisely controlling the focus position on the finger pad. However, the workspace has been limited to the vicinity of the phased array to secure the small focus on the finger and reproduce local shapes such as edges. In this study, to expand the workspace, we propose amplifying radiation force and enhancing local shape expression using a passive wearable attachment device based on a lever mechanism. The ultrasonic focus controls the contact position between the finger pad and the attachment device according to the finger's movement in real time, allowing the user to experience the amplified and enhanced sensation of stroking edges and curved surfaces. The results of the psychophysical experiment demonstrated that a curved surface with a curvature radius of 26.7 mm and an edge with an angle of 119.7 deg were presented at a position 500 mm away from the phased array with a long side of 384 mm.**

***Index Terms*—Edge, curved surface, passive haptic device, ultrasound**

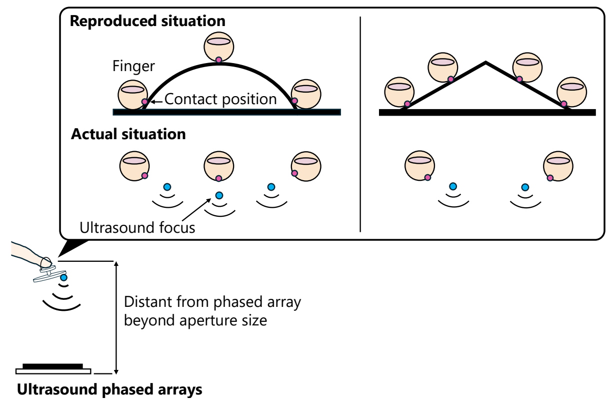

Fig. 1. Concept of the ultrasound-driven haptic device for presenting curved surface and edge. When an ultrasound focus is presented to the device, the device tilts, changing the contact position with the finger pad. By dynamically changing the contact position in response to the user's finger movements, stroking sensations of edges and curved surfaces are reproduced.

I. Introduction

Haptic reproduction of real object shapes is one of the key elements in haptic technology for realistic virtual reality (VR) content. By touching objects, we perceive the shape information that allows us to intuitively perform various tasks, including typing on a keyboard, pressing buttons, and manipulating objects. If characteristic object shapes such as edges and surface curvature can be reproduced using haptic devices, it enables efficient task performance through haptics in VR environments and enhances the realism of the VR experience. To that end, various shape presentation devices and techniques have been proposed [1]–[4]. Benko et al. developed a 3DoF controllable haptic disk. This device can control the contact position to the finger pad, rendering various curvature of curves [4].

Such local shapes can be displayed by ultrasound midair haptics [5]–[12]. Focusing ultrasound using a phased array generates a non-contact force by radiation pressure [13], which creates a local contact shape. Somei et al. demonstrated that moving the ultrasound focal point on a finger according to its movement can reproduce the sensation of stroking a curved surface [12]. This focus position was determined to replicate the actual change in contact position between the finger and a real curved surface. Since this method does not require the user to wear a device, it enables the presentation of curved surfaces without restricting the user's natural body motion.

However, since the radiation force by focused ultrasound is as weak as tens of millinewtons, the workspace for shape presentation using focus movement is limited to the proximity of an ultrasound phased array to secure the minimum necessary force. Furthermore, as the focus presentation distance exceeds the aperture length of the phased array, the focus becomes blurred, reducing its spatial resolution. With such weak and blurred stimuli, haptic reproduction of object shapes, such as curved surfaces, is difficult. To avoid this focus blur, Somei et al. conducted shape rendering only near the phased array [12]. The focus distance was approximately equal to the aperture length [12].

In this study, to expand the workspace for shape presentation, we propose amplifying radiation force and enhancing local shape expression using a passive wearable device based on the lever mechanism. The proposed concept is illustrated in Fig. 1. The attachment device on the finger is made of plastic and lightweight at 1.86 g, keeping the physical burden on the user low. Users wear this device so that a plastic curved plate fits their fingertips. When an ultrasound focus is

This work was supported in part by JST ACT-X JPMJAX21KJ and NEDO SIP 23201554-0.

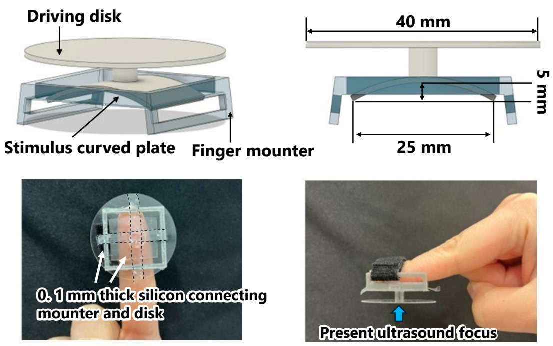

Fig. 2. Proposed device. When presenting ultrasound focus to the driving disk, the disk and the stimulus curved plate are tilted.

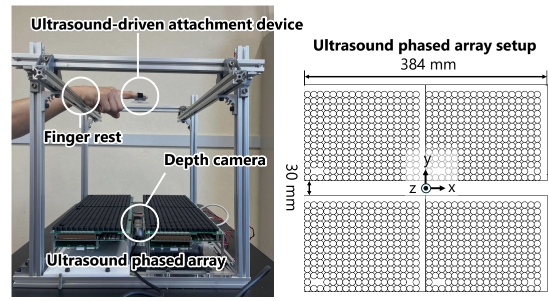

Fig. 3. The ultrasound-driven attachment device and driving system setup. Participants wore the attachment device on their index finger and placed it so that the driving disk faced the ultrasound phased array. The depth camera measured the device's 3D position.

presented to a disk connected to this curved plate, the curved plate tilts, changing the contact position with the fingertip. This disk acts as a lever, generating torque to drive the device according to the applied position of the focus. By dynamically changing the angle of the disk, i.e., the contact position of the curved plate with the fingertip, in response to the user's finger movements, stroking sensations of virtual curved surfaces can be reproduced.

In the experiment, we quantitatively evaluated that the developed haptic attachment device presents the stroking sensations of curved surfaces and sharp edges, even when positioned 500 mm (1.3 times the long side of the phased array) away from the phased array. By controlling the disk angle between -10 and 10 deg, a convex surface with a curvature radius of 26.7 mm was reproduced. Furthermore, by switching the angle between two discrete values, -10 and 10 deg, an edge with a 119.7 deg angle was reproduced.

Although some previous studies have proposed a similar approach, amplifying radiation force using passive mechanism [14], [15], no study reproduced the stroking sensation of curved surfaces and edges. Morisaki et al. amplified radiation force using a lever and presented a strong force of 0.7 N and low-frequency vibration below 30 Hz [14]. Kato et al. amplified radiation force using a thin-film device with a small pin [15], reproducing touch sensations of small protrusions.

Some studies have combined ultrasound phased array and physical objects to extend the workspace of ultrasound haptic; however, there is no study on local shape rendering. The use of a large concave acoustic reflector [16] and a robot arm manipulating a phased array [17], [18] have been proposed.

Actuators that are remotely driven using laser or magnetic force have also been proposed [19]–[24]. These devices do not focus on presenting haptic local shapes based on precise control of stimulation positions as our device.

II. Haptic attachment device rendering shape

A. Device and Driving System

This section introduces an overview of the proposed haptic display system. Fig. 2 shows a photograph and a schematic diagram of the developed haptic attachment device. This disk device consisted of the "stimulus curved plate," a 25 mm-wide curved plate with a curvature radius of 18.1 mm that contacts the skin to provide haptic stimulus; the "driving disk," a 40 mm-diameter disk, that receives ultrasound focus; and a mounting part for attaching the device to a finger. The driving disk was made of acrylic. The stimulus curved plate and the mounting part were fabricated using an optical 3D printer (Form3+, Formlabs). The material used for 3D printing was a resin with Young's modulus of 2.77 GPa (Formlabs Resin V4). The stimulus curved plate and driving disk were bonded rigidly. The driving disk and the mounting part were joined by an elastic rubber membrane with a thinness of 0.5 mm, allowing control of the driving disk angle by applying ultrasound focus.

Fig. 3 illustrates the driving system of the disk-shaped device. This system consists of a depth camera (RealSense D435, Intel) for tracking the 3D position of the haptic device and an ultrasound phased array for generating ultrasound focus [25] to drive the passive device. Color markers in red, blue, and green were attached to the driving disk, and the 3D positions of these markers were detected using binary color filters. The average of these 3D positions was treated as a position of the haptic device. Ultrasound phased array is an array of individually controllable ultrasound transducers. By appropriately controlling these phases, ultrasound focus is generated at arbitrary positions in midair, achieving the presentation of radiation force to the driving disk of the haptic device. In this study, 996 ultrasound transducers operating at 40 kHz were used [25].

B. Shape Rendering Method

The basic driving strategy of the attachment device is controlling the applied focus position on the driving disk. The angle of the stimulus curved plate changes by shifting the focal position on the driving disk, assuming the angle is proportional to the moment by the radiation pressure. As a result, the contact position between the finger pad and stimulus curved plate changes. Stroking sensation of curves and edges are presented by adjusting this contact position according to the movement of the finger in real time.

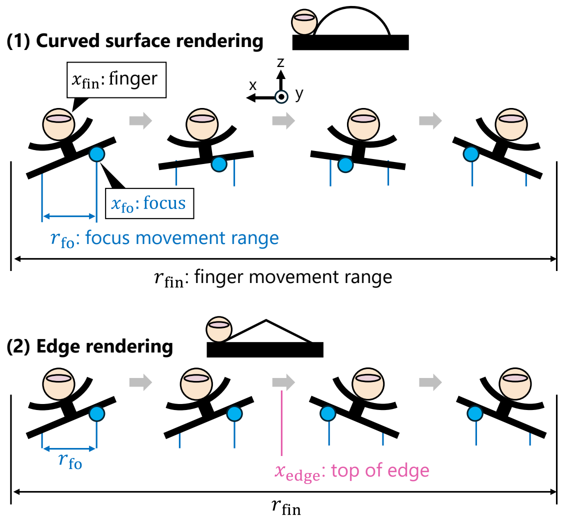

Fig. 4. A focus control algorithm for rendering edge and curved surface. Based on the relative position between a fingertip and a virtual surface, the focus position is horizontally moved. (1) In curved surface rendering, the focal point moves continuously in the opposite direction to the finger movements. (2) In edge rendering, the focus position switches between two positions, and the switch's position is the center of the virtual edge.

1) Curved surface: Fig. 4-1 shows a schematic of the focal position change pattern for presenting the stroking sensations of a curved surface. When a finger strokes horizontally a real curved surface, the contact position between the finger pad and the surface moves in the opposite direction to the finger's movement. To reproduce this change in the contact position, the focal position on the driving disk was moved opposite to the finger's movement. The angle of the stimulus curved plate was then gradually changed, resulting in movement of the contact position between the finger pad and the stimulus curved plate.

The focus x-position x_{fo} in the ground coordinate with respect to the finger x-position x_{fin} is formulated as follows:

$$x_{\mathrm{fo}} = -\frac{r_{\mathrm{fo}}}{r_{\mathrm{fin}}} x_{\mathrm{fin}} + x_{\mathrm{fin}}, \tag{1}$$

where r_{fo} and r_{fin} are the total distance of focus movement and finger movement. The r_{fin} corresponds to the width of the haptically rendered curved surface using the haptic attachment. The zero of the x-position corresponds to the center of the rendered curved surface.

In this method, the curvature of the presented surface is controlled with the total distance of focus movement r_{fo}. When stroking a surface with a large curvature radius, the contact position between the finger and the surface is largely moved by a small finger movement. When the curvature radius is small, this contact position displacement is small.

2) Edge: Fig. 4-2 shows a schematic of the focus position change pattern to present the stroking sensation of an edge. When stroking the edge horizontally with a finger, the contact point between the finger pad and the surface changes only when crossing the top of the edge. To reproduce this change in contact position, the focus position switched in only two stages: before and after crossing the edge.

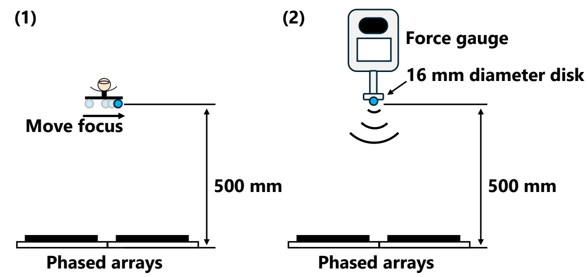

Fig. 5. Measurement setup. (1) Setup for measurement variation of driving disk angle. (2) Setup for measurement of the radiation force at focus. The radiation force was 13 mN (1.3 gf).

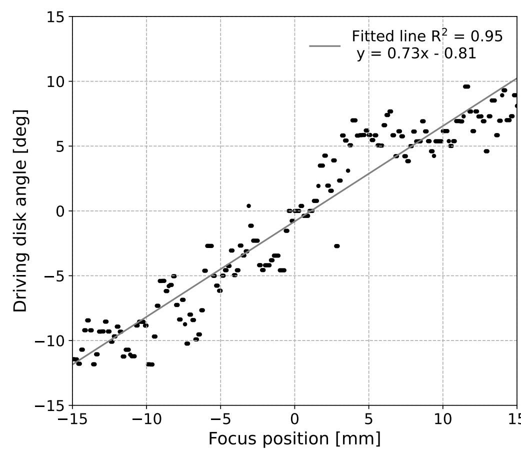

Fig. 6. Measurement result of driving disk angle variation with respect to horizontal focus movement. This data indicates that the angle linearly varies with respect to the focus position.

The x_{fo} with respect to the x_{fin} for rendering edge is formulated as follows:

$$x_{\mathrm{fo}} = \begin{cases} \frac{r_{\mathrm{fo}}}{2} + x_{\mathrm{fin}} & \text{if } x_{\mathrm{fin}} \leq x_{\mathrm{edge}}, \\ -\frac{r_{\mathrm{fo}}}{2} + x_{\mathrm{fin}} & \text{if } x_{\mathrm{fin}} > x_{\mathrm{edge}}. \end{cases} \tag{2}$$

where x_{edge} is the top position of the rendered edge.

The edge angle, i.e., edge sharpness, is controlled with r_{fo}, the distance of focus movement.

C. Physical Measurement

1) Driving disk angle: In this section, we measured the actual angle variation of the driving disk when horizontally moving the focus position.

Fig. 5-1 illustrates the experimental setup. The device was attached to the author's finger and positioned at the center of the phased arrays. The distance between the device and the phased arrays was 500 mm. To stabilize, the finger was placed on a finger rest as shown in Fig. 3. A focus was presented at $x_{\mathrm{fo}} = -15$ mm, then horizontally shifted to $x_{\mathrm{fo}} = 15$ mm by

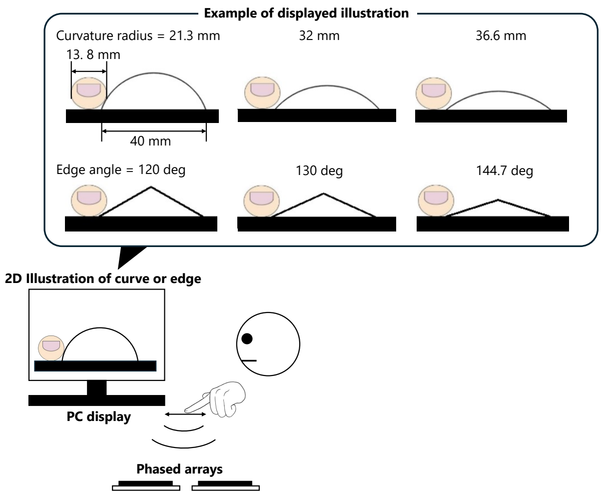

Fig. 7. Experimental setup for evaluating perceived curvature and edge angle (sharpness). Participants experienced haptic stimulus and compared its curvature/edge angle with a 2D illustration of a curved surface/edge.

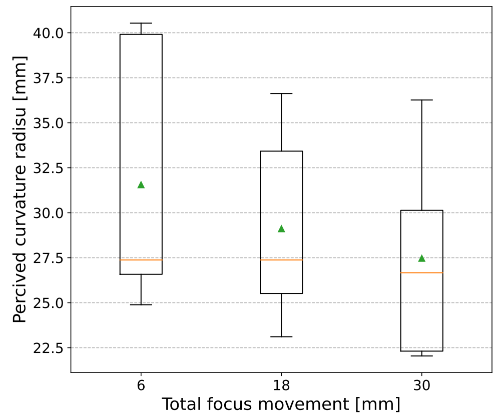

Fig. 8. Evaluation result of perceived curvature radius. The perceived curvature radius has significantly decreased as the focus movement increased.

0.1 mm every 10 ms. The disk angle was measured using the depth camera.

The measurement result is shown in Fig. 6. We fitted a linear function to the measurement data. The fitting result shows that the driving disk angle θ is described as follows:

$$\theta = 0.73x_{\mathrm{fo}} - 0.81. \tag{3}$$

The R^2 coefficient of determination was 0.95.

The regression result indicated that the driving disk angle was linearly changed for the focus movement.

2) Radiation force: We measured the radiation force at the ultrasound focus and the force was 13 mN (1.3 gf). The measurement setup is illustrated in Fig. 5-2. The focus was created at the center of the phased array. The focus distance from the phased array was 500 mm, which was the same as in other experiments. A 16 mm diameter plastic disk was placed at the focus position, and the applied force was measured by a digital force gauge (ZTS-5N, IMADA). The disk size was chosen to cover the entire focus.

III. Evaluation of Haptic Shape Rendering

We evaluated the changes in the perceived curvature and edge angle when the angle of the driving disc changes.

A. Curved surface

1) Procedure: In this experiment, we presented a stroking sensation of curved surfaces using the attachment device and evaluated the perceived curvature. The curvature was quantified by comparing it with a 2D illustration of curved surfaces. Seven males and a female (mean age: 25.6 years, 7 males, 1 female) participated in the experiment. All procedures were performed in accordance with the Declaration of Helsinki (2008), and participants provided written informed consent prior to the commencement of the experiments.

The experimental setup is shown in Fig. 7. First, participants wore the passive haptic attachment display on their fingers and positioned it 500 mm away from the phased array. They moved their finger horizontally from $x_{\mathrm{fin}} = 20$ mm to $x_{\mathrm{fin}} = -20$ mm only once. A marker was displayed on the PC display horizontally moving at 20 mm/s, and participants were instructed to move their fingers at the same speed as the marker. The focus position for the finger position was calculated using eq. 1 with the total focus movement $r_{\mathrm{fo}} = 30, 18, 6$ mm. The three r_{fo} were used in random order. Next, an illustration of a curved surface was visually shown to participants on a PC display. We calibrated the PC display so that the illustration was displayed at the desired size. The initial curvature radius of the illustration was 21.3 mm. The illustrated curvature was varied with the staircase method. The initial order was ascending order. This initial curvature was empirically chosen through preliminary experiments. Participants compared the presented haptic stimulus with the illustration and answered which had the higher curvature radius. If they answered that the curvature radius of the haptic stimulus was high, the curvature radius of the illustration was increased by 1.07 mm. Afterward, the haptic stimulus was presented, and participants compared it with the illustration again. This increased process continued until the illustration's curvature radius was higher, i.e., the participant's response was reversed. The curvature radius was continuously decreased until the response reversed again. These curvature comparison processes were repeated until six response reversals were gained. The curvature radius of the illustration at each reversal was recorded, and their average was taken as the perceived curvature. All participants successfully completed the task, and no experimental data were excluded.

2) Result: The evaluation results of the perceived curvature radius are shown in Fig. 8. The median value of the perceived curvature radius was 27.4, 27. 4, and 26.7 mm for total focus movement r_{fo} of 6, 18, 30 mm.

We analyze the effect of r_{fo} with a significance level of

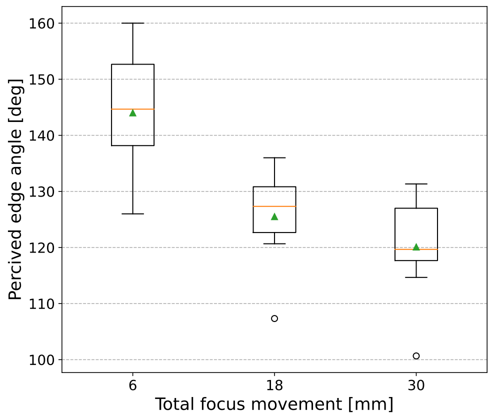

Fig. 9. Evaluation result of perceived edge angle. The perceived edge angle significantly decreased as the focus movement increased.

0.05. The Shapiro-Wilk test indicates that the curvature data for $r_{\mathrm{fo}} = 30$ mm was not normally distributed. Although the data for $r_{\mathrm{fo}} = 6, 18$ mm were normally distributed, we used nonparametric analysis. We applied the Friedman test to the curvature data. The result indicated that the total focus movement r_{fo} has a significant effect on the perceived curvature ($p = 0.0087$). As a post-hoc test, we applied the Wilcoxon signed-rank test with Bonferroni-Holm Correction to the data. The significant difference was observed in the r_{fo} pair of [6 and 30 mm ($p = 0.046$)]. We also calculated effect size $r = \frac{z}{\sqrt{N}}$, where z is the z statistic value and N is the measurement number. The effect size r was 0.385, 0.592, and 0.385 of the r_{fo} pair of [6 and 18 mm], [6 and 30 mm], and [18 and 30 mm], respectively.

The evaluation results and the statistical analysis indicated that the perceived curvature radius was significantly decreased as the total focus movement r_{fo} increased.

B. Edge

1) Procedure: We presented a stroking sensation of an edge and evaluated its angle (sharpness). The participants in this experiment were the same as the curved surface experiment.

The experimental setup and procedure are shown in Fig. 7. The procedure was the same as the curved surface experiment. The focus position for the finger position was calculated using eq. 2 with the total focus movement $r_{\mathrm{fo}} = 30, 18, 6$ mm. The edge top position was $x_{\mathrm{edge}} = 0$ mm. Participants experienced a haptic stimulus and compared its sharpness with that of the edge illustration shown on a PC display. The sharpness (edge angle) of the illustration varied by 2 deg using a staircase method. The initial angle was 120 deg, and the initial order was ascending. The edge angle of the illustration at each participant's response reversal was recorded, and their average was taken as the perceived edge angle. All participants successfully completed the task, and no experimental data were excluded.

2) Result: The evaluation results of the edge angle are shown in Fig. 9. The median value of the perceived angle was 144.7, 127.3, 119.7 for r_{fo} of 6, 18, 30 mm.

We analyze the effect of r_{fo} with a significance level of 0.05. Since the Shapiro-Wilk test indicates that all edge data was normally distributed, we used parametric analysis. We applied the repeated measures ANOVA to the edge data. The result indicated that r_{fo} has a significant effect on the perceived edge angle ($p = 0.004$). As a post-hoc test, we applied the paired t-test to the data with Bonferroni-Holm Correction. The significant difference was observed in the r_{fo} pair of [6 and 18 mm ($p = 0.033$)], [6 and 30 mm ($p = 0.006$)], and [18 and 30 mm ($p = 0.046$)]. The effect size of Cohen's d was 1.88, 2.33, and 0.58 of the r_{fo} pair of [6 and 18 mm], [6 and 30 mm], and [18 and 30 mm], respectively.

The evaluation results and the statistical analysis indicated that the perceived edge angle was significantly decreased as the total focus movement r_{fo} increased.

IV. Discussion

A. Perceived shape

The experimental results indicated that the developed haptic device can render a curved surface with a curvature radius of 27.5 mm and an edge with an angle of 120 deg, even at a distance of 500 mm from the phased array. The results shown in Fig. 8 and Fig. 9 indicate that the perceived edge angle and perceived curvature shifted according to the focal movement distance, i.e., the driving disk angle. This suggests that the participants perceived the edges and curved surfaces. The analysis results also showed that the focus movement distance r_{fo} had a significant effect on the perceived curvature and edge angle.

It was also shown that edges were perceived more clearly than curved surfaces. In the curved surface presentation, the variance in perceived curvature was large, and only one r_{fo} pair had significant differences. In contrast, in the edge presentation, significant differences were observed between all conditions. The stability of edge perception would be achieved by using a simple two-step focal movement for edge presentation. The curved surface presentation required continuous focal movement, which may have made perception more difficult.

B. Simulation of rendered shape

This section simulated the curvature radius of curved surfaces and the angles of edges that the haptic attachment device can render.

The simulation setup is shown in Fig 10-1. The stimulus curved plate was modeled as an arc. The chord length was 25 mm and the curvature radius was 18.1 mm, matching the actual experimental setup. A finger was modeled as a circle with a radius of r_{s1} = 10, 12, and 14 mm. The maximum radius of 14 mm was chosen to simulate a situation where the finger fits well with the stimulus curved plate.

The simulation procedure is shown in Fig 10-1. First, the arc was placed 10 mm below the circle. Then, the arc was rotated

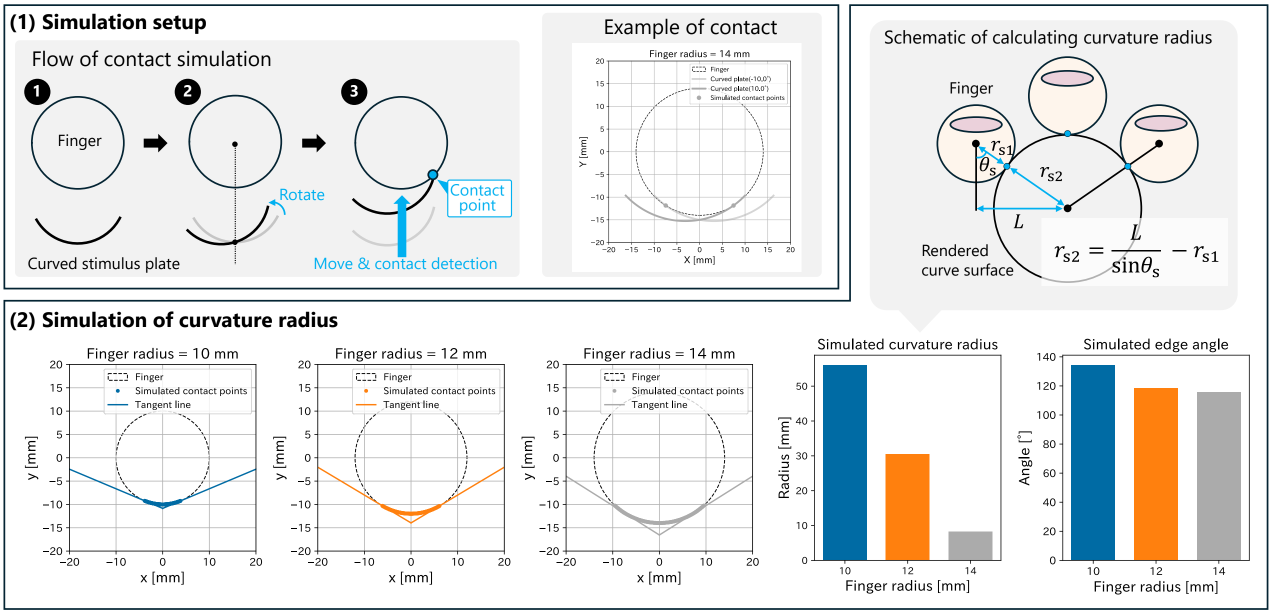

Fig. 10. Simulation of rendered curved surface and edge. (1) Simulation setup. A finger was modeled as a circle with a radius of 10, 12, and 14 mm. The curved stimulus plate was modeled as an arc with a curvature of 18.1 mm. (2) Simulation results and schematic of calculating curvature radius. The arc angle was varied from -10 deg to 10 deg.

around its center, and the y-position of the arc was increased by 0.01 mm until it came into contact with the circle. For contact detection, the arc was sampled at 0.35 µm intervals. The distance between the sampled points and the center of the circle was calculated in each movement step of the arc. All sampled points where the calculated distance was less than 0.1 mm were gained and the average of the gained points was finally considered as the contact point.

Fig. 10-2 shows the variation in the contact position and the simulated curvature radius. The curvature radius was 56.1, 30.6, and 8.2 mm for $r_{s1} = 10, 12, 14$ mm, respectively. The arc rotated from -10 to 10 deg. The curvature radius r_{s2} was calculated as follows:

$$r_{s2} = \frac{L}{\sin\theta_s} - r_{s1}, \tag{4}$$

where L is half of the horizontal movement distance of the finger (circle), set to 20 mm as in the experiment. θ_s is the angle between the contact point and the y-axis at the arc angle of -10 deg.

Fig. 10-2 shows the simulated edge angle. The angle was 134.5, 118.2, and 96.8 deg for $r_{s1} = 10, 12, 14$ mm, respectively. First, the tangent at the contact point with the arc angle of -10 deg was calculated. The simulated edge angle was twice as much as the angle between the tangent and y-axis.

These simulation results indicated that our haptic attachment device was appropriately driven with a device-finger roughly fit condition. The middle value of the simulated curvature radius was 30.4 mm, matching the perceived minimum radius of 26.7 mm. The middle value of the simulated edge angle was 118.2 deg, matching the perceived minimum angle of 119.7 deg.

C. Limitation and Future work

We did not evaluate the actual shapes the participants perceived. We will ask participants to draw a perceived shape.

The driving algorithm of the haptic attachment using Eq. 1 and 2 was limited to rendering a simple curved surface and edge. We will extend the driving algorithm to render more complex shapes, such as multiple curved surfaces.

In the curvature evaluation, a significant difference was detected in only one r_{fo} pair. This is because the effect size was medium and lower than we expected. We will redesign the sample size based on this effect size.

V. Conclusion

In this study, we proposed an ultrasound-driven haptic shape display and demonstrated that the device can render edges and curved surfaces even at a distance from an ultrasound phased array. This device rendered these shapes by dynamically changing the contact angle between the finger pad and a plastic curved plate according to the finger movement. Its driving force was the ultrasound radiation force amplified by a lever, achieving the large workspace of shape rendering.

In the experiment, we quantified the perceived curvature and edge angles. This evaluation was conducted 500 mm away from a phased array with a long side of 384 mm. The smallest perceived curvature radius was 26.7 mm, and the sharpest perceived edge angle was 119.7 deg.

In future works, we will present haptic textures using the ultrasound-driven haptic display by rendering multiple aligned edges or curved surfaces.

REFERENCES

[1] M. W. Wijntjes, A. Sato, V. Hayward, and A. M. Kappers, "Local surface orientation dominates haptic curvature discrimination," *IEEE transactions on haptics*, vol. 2, no. 2, pp. 94–102, 2009.

[2] M. Solazzi, A. Frisoli, and M. Bergamasco, "Design of a novel finger haptic interface for contact and orientation display," in *2010 IEEE Haptics Symposium*. IEEE, 2010, pp. 129–132.

[3] D. Prattichizzo, F. Chinello, C. Pacchierotti, and M. Malvezzi, "Towards wearability in fingertip haptics: a 3-dof wearable device for cutaneous force feedback," *IEEE Transactions on Haptics*, vol. 6, no. 4, pp. 506–516, 2013.

[4] H. Benko, C. Holz, M. Sinclair, and E. Ofek, "Normaltouch and texturetouch: High-fidelity 3d haptic shape rendering on handheld virtual reality controllers," in *Proceedings of the 29th annual symposium on user interface software and technology*, 2016, pp. 717–728.

[5] T. Hoshi, M. Takahashi, T. Iwamoto, and H. Shinoda, "Noncontact tactile display based on radiation pressure of airborne ultrasound," *IEEE Transactions on Haptics*, vol. 3, no. 3, pp. 155–165, 2010.

[6] T. Carter, S. A. Seah, B. Long, B. Drinkwater, and S. Subramanian, "Ultrahaptics: multi-point mid-air haptic feedback for touch surfaces," in *Proceedings of the 26th annual ACM symposium on User interface software and technology*. ACM, 2013, pp. 505–514.

[7] B. Long, S. A. Seah, T. Carter, and S. Subramanian, "Rendering volumetric haptic shapes in mid-air using ultrasound," *ACM Transactions on Graphics (TOG)*, vol. 33, no. 6, pp. 1–10, 2014.

[8] T. Howard, G. Gallagher, A. Lécuyer, C. Pacchierotti, and M. Marchal, "Investigating the recognition of local shapes using mid-air ultrasound haptics," in *Proceedings of 2019 IEEE World Haptics Conference (WHC)*. IEEE, 2019, pp. 503–508.

[9] A. Matsubayashi, H. Oikawa, S. Mizutani, Y. Makino, and H. Shinoda, "Display of haptic shape using ultrasound pressure distribution forming cross-sectional shape," in *Proceedings of 2019 IEEE World Haptics Conference*. IEEE, 2019, pp. 419–424.

[10] J. Martinez, A. Harwood, H. Limerick, R. Clark, and O. Georgiou, "Mid-air haptic algorithms for rendering 3d shapes," in *2019 IEEE International Symposium on Haptic, Audio and Visual Environments and Games (HAVE)*. IEEE, 2019, pp. 1–6.

[11] L. Mulot, T. Howard, S. Emery, C. Pacchierotti, and M. Marchal, "Designing 3d object rendering techniques for ultrasound mid-air haptics using intersection strategies," in *ACM Symposium on Applied Perception 2024*, 2024, pp. 1–8.

[12] Z. Somei, T. Morisaki, Y. Toide, M. Fujiwara, Y. Makino, and H. Shinoda, "Spatial resolution of mesoscopic shapes presented by airborne ultrasound," in *International Conference on Human Haptic Sensing and Touch Enabled Computer Applications*. Springer, 2022, pp. 243–251.

[13] K. Yosioka and Y. Kawasima, "Acoustic radiation pressure on a compressible sphere," *Acta Acustica united with Acustica*, vol. 5, no. 3, pp. 167–173, 1955.

[14] T. Morisaki, T. Kamigaki, M. Fujiwara, Y. Makino, and H. Shinoda, "Ultlever: Ultrasound-driven passive haptic actuator based on amplifying radiation force using a simple lever mechanism," *IEEE Transactions on Haptics*, 2024.

[15] K. Kato, D. Kon, K. Ueda, C. S. Dos Reis, N. Ienaga, and Y. Kuroda, "Enhanced haptic perception of virtual protrusions using a focused ultrasound-driven thin-film actuator," *IEEE Access*, 2024.

[16] K. Ariga, M. Fujiwara, Y. Makino, and H. Shinoda, "Workspace evaluation of long-distance midair haptic display using curved reflector," in *2021 IEEE World Haptics Conference (WHC)*. IEEE, 2021, pp. 85–90.

[17] S. Villa, S. Mayer, J. Hartcher-O'Brien, A. Schmidt, and T.-K. Machulla, "Extended mid-air ultrasound haptics for virtual reality," *Proceedings of the ACM on Human-Computer Interaction*, vol. 6, no. ISS, pp. 500–524, 2022.

[18] T. Howard, G. Gicquel, M. Marchal, A. Lécuyer, and C. Pacchierotti, "Pumah: Pan-tilt ultrasound mid-air haptics," in *WHC 2021-IEEE World Haptics Conference*, 2021, p. 1.

[19] D. Avirovik, A. Kumar, R. J. Bodnar, and S. Priya, "Remote light energy harvesting and actuation using shape memory alloy—piezoelectric hybrid transducer," *Smart Materials and Structures*, vol. 22, no. 5, p. 052001, 2013.

[20] T. Hiraki, K. Nakahara, K. Narumi, R. Niiyama, N. Kida, N. Takamura, H. Okamoto, and Y. Kawahara, "Laser pouch motors: Selective and wireless activation of soft actuators by laser-powered liquid-to-gas phase change," *IEEE Robotics and Automation Letters*, vol. 5, no. 3, pp. 4180–4187, 2020.

[21] S. Ueno and Y. Monnai, "Wireless soft actuator based on liquid-gas phase transition controlled by millimeter-wave irradiation," *IEEE Robotics and Automation Letters*, vol. 5, no. 4, pp. 6483–6488, 2020.

[22] P. Berkelman, M. Miyasaka, and J. Anderson, "Co-located 3d graphic and haptic display using electromagnetic levitation," in *2012 IEEE Haptics Symposium (HAPTICS)*. IEEE, 2012, pp. 77–81.

[23] M. Weiss, C. Wacharamanotham, S. Voelker, and J. Borchers, "Fingerflux: near-surface haptic feedback on tabletops," in *Proceedings of the 24th annual ACM symposium on User interface software and technology*, 2011, pp. 615–620.

[24] X. Lu, Y. Yan, B. Qi, H. Qian, J. Sun, and A. Quigley, "Contactless haptic display through magnetic field control," *IEEE Transactions on Haptics*, 2022.

[25] S. Suzuki, S. Inoue, M. Fujiwara, Y. Makino, and H. Shinoda, "Autd3: Scalable airborne ultrasound tactile display," *IEEE Transactions on Haptics*, vol. 14, no. 4, pp. 740–749, 2021.